Cu and Fe oxides dispersed on SBA-15: A Fenton type bimetallic catalyst for *N,N*-diethyl-*p*-phenyl diamine degradation

S. Karthikeyan [a,c], M.P. Pachamuthu [b], Mark A. Isaacs [a], Santosh Kumar [a], Adam F. Lee [a,*], G. Sekaran [c,*]

[a] *European Bioenergy Research Institute, Aston University, Aston Triangle, Birmingham B4 7ET, United Kingdom*
[b] *Department of Chemistry, Bannari Amman Institute of Technology, Sathyamangalam, Tamil Nadu 638 401, India*
[c] *Environmental Technology Division, Central Leather Research Institute, Adyar, Chennai 600 020, India*

ARTICLE INFO

ABSTRACT

A bimetallic oxidation catalyst has been synthesized via wet impregnation of copper and iron over a mesoporous SBA-15 silica support. Physicochemical properties of the resulting material were characterized by XRD, N_2 physisorption, DRUVS, FTIR, Raman, SEM and HRTEM, revealing the structural integrity of the parent SBA-15, and presence of highly dispersed Cu and Fe species present as CuO and Fe_2O_3. The CuFe/SBA-15 bimetallic catalyst was subsequently utilized for the oxidative degradation of *N,N*-diethyl-*p*-phenyl diamine (DPD) employing a H_2O_2 oxidant in aqueous solution.

© 2016 The Author(s). Published by Elsevier B.V. This is an open access article under the CC BY license (http://creativecommons.org/licenses/by/4.0/).

1. Introduction

Water pollution remains a major challenge for emergent countries due to the ongoing unregulated discharge of toxic and non-biodegradable chemicals into aquatic environments [1–4], which conventional wastewater treatment methods, including biological microorganism and/or physico-chemical processes (flocculation, chlorination and ozonation), are unable to effectively remove [5,6]. Existing water remediation technologies thus require additional post-treatments to avoid secondary disposal issues and contamination [7]. Advanced oxidation processes (AOPs) are promising alternative technologies for the removal of toxic-and non-biodegradable compounds in water [7–11], operating at ambient temperature and pressure to generate strongly oxidizing hydroxyl radicals (•OH) able to completely degrade organic compounds into non-toxic products (ideally CO_2 and H_2O) [11–13]. Amongst the different AOPs, Fenton reactions based around iron redox chemistry has gained popularity due to high removal efficiencies for recalcitrant organic contaminants, in addition to the natural abundance of iron, ease of catalyst separation and low cost [14].

Heterogeneous Fenton type AOPs have attracted much recent attention [15], and have the potential to combat diverse acidic, basic and neutral pollutants discharged into the environment [16–18]. Mesoporous inorganic solids such as MCM, SBA, KIT and TUD materials offer great opportunities across materials science. However, there are few reports on the use of ordered mesoporous silicas for heterogeneous Fenton oxidation [19–22]. One of the most widely utilized such ordered, mesoporous silicas, SBA-15, exhibits a high specific surface area, tunable pore size, narrow pore size distribution, and hydrothermal stability, rendering it very attractive for catalysis, adsorption, bio-sensing, and controlled drug delivery [12,14,23,24]. SBA-15 facilitates the genesis of isolated metal ions (M^+), the dispersion of metal oxide (M_xO_y) and metal (M^0) nanoparticles, and a broad range of organic functionalities. Bimetallic systems comprising copper in combination with iron have shown promise for a wide range of heterogeneously catalyzed reactions including borane hydrolysis for hydrogen production [25], phenol [19] and toluene oxidation [26], and heterogeneous Fenton degradation of phenolics [27,28] and dyes such as Rhodamine B [29]. In many of these systems iron leaching and concomitant catalyst deactivation was reported. An important but little studied neutral amine *N,N*-diethyl-*p*-phenyl diamine (DPD) is used widely in color photography, as a dye intermediate, rubber component, and reducing agent in the petrochemical industry [30,31] and its discharge into water streams can cause allergic dermatitis in humans [32]

---

* Corresponding authors.
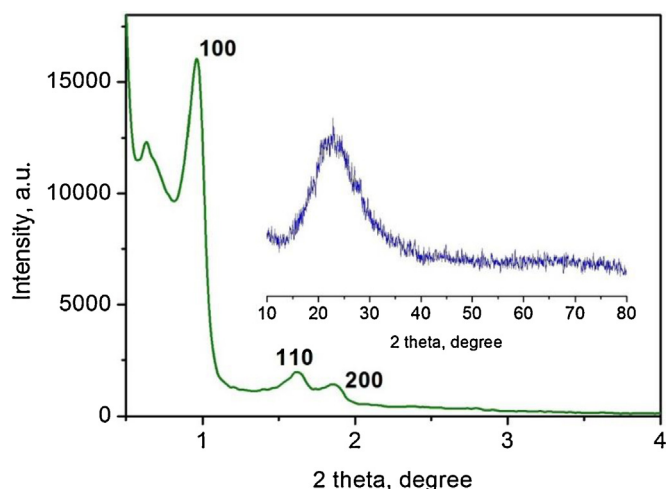 *E-mail address:* ganesansekaran@gmail.com (G. Sekaran).

Fig. 1. Low angle and (inset) wide angle XRD patterns of CuFe/SBA-15.

We reported recently DPD degradation using a FeTUD-1 catalyst, which afforded reductions of 91% of COD and 80% of TOC under mild reaction conditions [31]. Herein, we report a simple preparative route to a bimetallic CuFe/SBA-15 catalyst, comprising highly dispersed Cu and Fe oxides for the Fenton-like oxidation of DPD in aqueous solution under mild conditions in which synergy between the transition metals confers excellent degradation performance.

2. Experimental

2.1. Catalyst synthesis

SBA-15 was synthesized using Pluronic P123 ($EO_{20}PO_{70}EO_{20}$) as a mesopore template and tetraethylorthosilicate (TEOS) as the silica source under acidic conditions similar to that reported by Shylesh and Singh [33]. Briefly, 2 g of P123, 15 g water and 60 g of 2 M HCl were mixed at 35 °C to yield a homogenous mixture. After stirring for 30 min, 4.25 g of TEOS was added gradually and stirring continued for 24 h. The obtained mixture was transferred and sealed in a Teflon autoclave for hydrothermal treatment at 100 °C for 24 h. The resulting gel was filtered off and washed with distilled water before drying at 100 °C for 12 h to yield a solid powder. Template removal was performed by calcination at 550 °C for 6 h under air resulting in the final SBA-15 support. CuFe/SBA-15 sample was prepared by incipient wetness impregnation of the mesoporous silica with an aqueous mixture of 75 mg copper nitrate ($Cu(NO_3)_2 \cdot 3H_2O$) and 74 mg iron nitrate ($Fe(NO_3)_2 \cdot 9H_2O$) salts as the Cu and Fe oxide sources respectively. Monometallic Cu/SBA-15 and Fe/SBA-15 analogues were likewise prepared through incipient wetness impregnation with each precursor. Individual Cu and Fe loadings were approximately 4 wt% in the bimetallic and monometallic samples, which were subsequently dried at 100 °C for 12 h prior to calcination in air at 500 °C for 4 h.

2.2. Catalyst characterization

Powder X-ray diffractograms ($2\theta = 0.5-6°$ and $2\theta = 10-80°$) of the sample were recorded on a Bruker D8 diffractometer using Cu Kα radiation ($\lambda = 1.5418$ Å). Nitrogen adsorption and desorption isotherm was obtained at 77 K using a Micromeritics ASAP 2020 porosimeter. Prior to the experiments, the sample was degassed under vacuum at 473 K for 3 h. The specific surface area and pore size distribution of the sample was calculated using the BET method and BJH method respectively (using the adsorption isotherm). Diffuse reflectance UV–vis spectroscopy (DRUVS) was recorded in the range 200–800 nm with a Perkin Elmer spectrometer using a $BaSO_4$ reference. FTIR of the CuFe/SBA-15 sample was recorded on a Bruker Tensor27 instrument at room temperature with a resolution of 4 cm^{-1}. Raman spectroscopy was performed on a Bruker FT-Raman 1000 R instrument using 1064 nm excitation. The morphology of the CuFe/SBA-15 was explored by scanning electron microscope (SEM, Quanta 200 FEG) with samples simply dispersed over carbon tape and not gold-coated. Bulk elemental analysis was performed by energy dispersive X-ray spectroscopy (EDX). High resolution transmission electron microscopy (HRTEM) was carried out on a JEOL 3010 instrument with a UHR pole piece (accelerating voltage of 300 kV). X-ray photoelectron spectroscopy (XPS) was acquired on a Kratos AXIS HSi spectrometer equipped with a charge neutralizer and monochromated Al Kα excitation source (1486.7 eV), with energies referenced to adventitious carbon at 284.6 eV. Spectral fitting was performed using CasaXPS version 2.3.14.
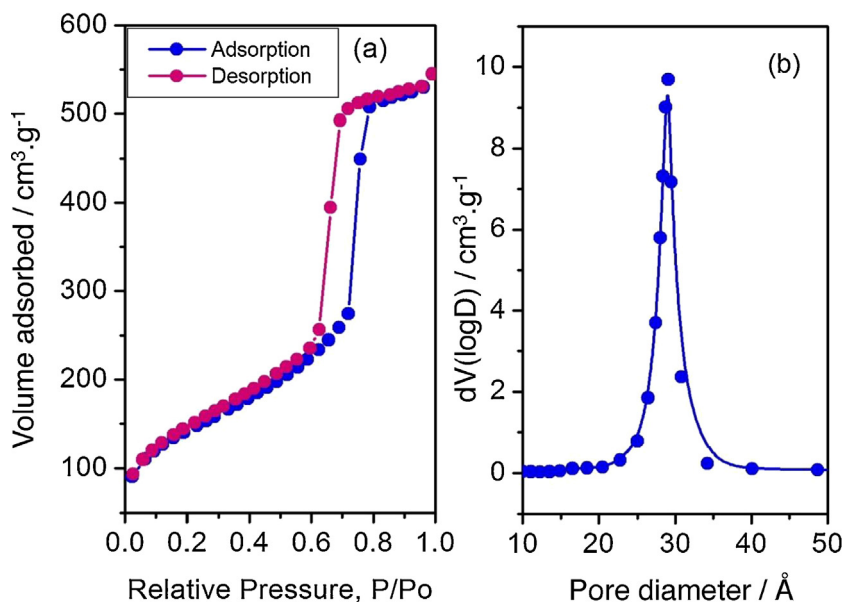

Fig. 2. (a) N$_2$ adsorption-desorption isotherms, and (b) BJH pore size distributions of CuFe/SBA-15.
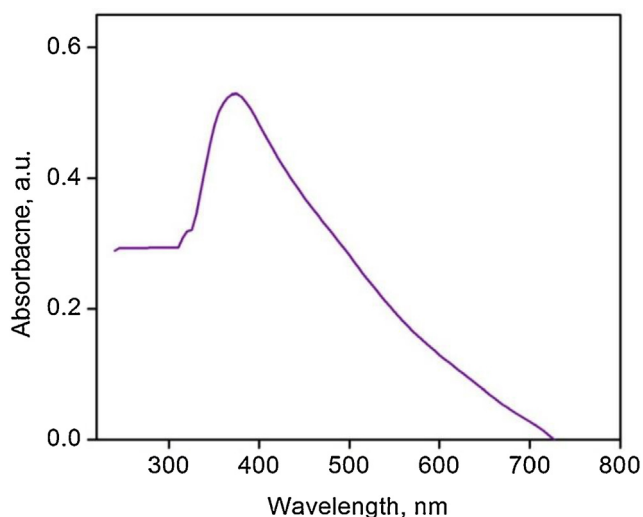
Fig. 3. DRUVS spectrum of CuFe/SBA-15 catalyst.

2.3. N,N-diethyl-p-phenyl diamine adsorption over cuFe/SBA-15

In the heterogeneously catalyzed degradation of organic pollutants, the latters' adsorption from aqueous solution plays a critical role. *N,N*-diethyl-*p*-phenyl diamine (DPD) adsorption was therefore performed by adding a fixed catalyst loading (0.5 g/L) to DPD solutions of varying concentrations between 0.1 g/L to 0.5 g/L, and the resulting slurries then placed in an orbital shaker for 24 h at 150 rpm and 27 °C until equilibrium was attained as determined from the characteristic 240 nm UV–vis absorbance. The amount of DPD adsorbed over CuFe/SBA-15 at equilibrium, q_e (in milligrams per gram), was obtained from Eq. (1),

$$q_e = (C_0 - C_e)V/W \tag{1}$$

where C_0 and C_e (in milligrams per liter) are the initial and equilibrium concentration of DPD, V is the volume of solution (in liters), and W is the mass of CuFe/SBA-15 (in grams).

2.4. N,N-diethyl-p-phenyl diamine degradation over CuFe/SBA-15

DPD degradation was conducted isothermally in a 250 mL polypropylene container employing 100 mL of stock solution (500 mg/L DPD in distilled water) with 8 mmol of H_2O_2 (50 vol%). A range of CuFe/SBA-15 catalyst charges were subsequently added to this solution, and aliquots periodically withdrawn during the course of reaction for subsequent UV–vis and total organic content (TOC) analysis[8] using a Perkin Elmer UV–vis spectrophotometry and Shimadzu–VCSH TOC analyzer. The extent of TOC removal was calculated from Eq. (2),

$$\%TOC\ removal = (TOC_{initial} - TOC_{final}) \times 100/TOC_{initial} \tag{2}$$

where TOC_{intial} and TOC_{final} (mg/L) are the initial and final DPD concentrations. Some of the degraded products were determined by HPLC (Shimadzu) using a C18 column (Phenomenex Luna 5 μ, C18 (2), 100 Å) detector UV 254 nm (acetonitrile + phosphate buffer eluent). A Micromass QuattroII triple quadrupole ESI LC–MS system was also used to identify the degraded products in positive ionization mode, details provided in the supporting information.

3. Results and discussion

3.1. Catalyst characterization

Low and wide angle XRD patterns of the as-prepared CuFe/SBA-15 catalyst are displayed in Fig. 1. The low angle diffractogram exhibits (100), (110) and (200) reflections characteristic of the *p6mm* SBA-15 ordered hexagonally close-packed support architecture [21,28,33,34]. The corresponding wide angle pattern (Fig. 1 insert) only exhibits a broad peak between 15° and 30° due to amorphous silica, with no reflections associated with copper or iron phases, indicating that these elements must be present in structures with dimensions below the size limit for detection, i.e. below approximately 2 nm, and hence are highly dispersed [28].

Nitrogen adsorption-desorption isotherms and corresponding pore size distributions of the CuFe/SBA-15 are shown in Fig. 2a,b (and of the parent SBA-15 in Fig. S1a,b), exhibiting a type IV isotherm with a H1-type hysteresis loop characteristic of mesoporous materials [34]. The high degree of mesopore ordering results in a sharp inflection at relative pressures (P/Po) between
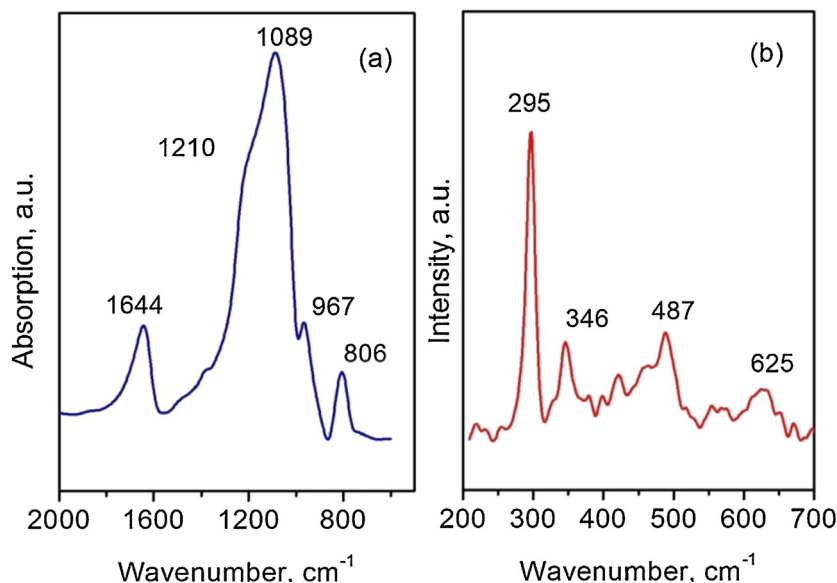

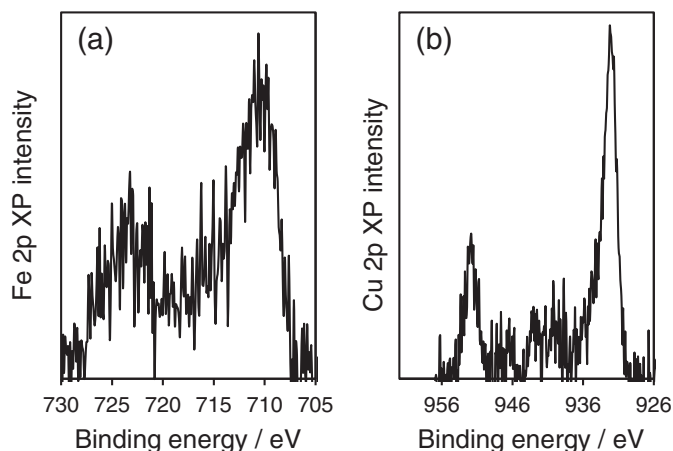**Fig. 4.** (a) FTIR and (b) FT-Raman spectra of CuFe/SBA-15 catalyst.

Fig. 5. (a) Fe and (b) Cu 2p XP spectrum of background-subtracted CuFe/SBA-15 catalyst.

0.6 and 0.8, consistent with well-defined 3 nm mesopores and evidencing retention of the parent SBA-15 mesostructure. The BET surface area and pore volume of CuFe/SBA-15 was 596 m^2/g and 0.75 cm^3/g, similar to that of the parent SBA-15 (650 m^2/g) and hence demonstrating minimal pore blockage following transition metal impregnation.

A broad absorption peak maximum was observed at 370 nm in the DRUV spectrum of the CuFe/SBA-15 sample (Fig. 3) which is assigned to the presence of CuO and Fe$_2$O$_3$ clusters [35]. Notably, there were no higher wavelength (>400 nm) absorbances due to bulk oxides, indicative of a high copper and iron dispersion, consistent with the wide angle XRD in Fig. 1.

The FT-IR and FT-Raman spectra of CuFe/SBA-15 sample are shown in Fig. 4a,b. The IR spectrum shows an absorption band at 1644 cm^{-1} attributed to the bending mode of adsorbed water, with intense bands at 1210, 1089 and 806 cm^{-1} arising from Si—O—Si asymmetric and symmetric stretching modes[21]. The Raman spectrum exhibits peaks at 295, 346, 487 and 625 cm^{-1}, which those at 295, 346 and 625 cm^{-1} attributed to the A$_g$ and B$_g$ modes of CuO[35], with that at 487 cm^{-1} attributed to Fe$_2$O$_3$.

Surface elemental analysis by XPS revealed Cu and Fe loadings of 0.1 and 0.3 atom% (0.3 wt% and 0.7 wt%) respectively. The Fe 2p$_{3/2}$ XP binding energy of 710.55 eV (Fig. 5a) was consistent with the presence of Fe$_2$O$_3$ [36], although the low signal intensity prohibited clear observation of the anticipated shake-up satellite around 719 eV. The corresponding Cu 2p XP spectrum (Fig. 5b) exhibited a 2p$_{3/2}$ state around 932.3 eV, accompanied by a satellite at 240.6 eV, consistent with the presence of CuO[8]. Fig. 6a,b shows the SEM image and EDX profile of the CuFe/SBA-15 sample. As previously reported for SBA-15, uniform micron sized SiO$_2$ particle morphologies were observed (Fig. 6a), while EDX (Fig. 6b) confirmed the presence of Cu and Fe with bulk loadings of 2.93 and 1.72 wt.% respectively.

HRTEM in Fig. 7a,b visualize the expected close-packed hexagonal arrangement of parallel mesopores characteristic of the *p6mm* space group. The average wall thickness was ~3–4 nm, with similar width pore diameters in agreement with N$_2$ porosimetry. However, due to the low metal loadings and contrast it was difficult to clearly identify the transition metal oxide phases, in accordance with the highly dispersed species implied by XRD and DRUVS.

3.2. N,N-*diethyl*-p-*phenyl diamine adsorption*

Adsorption isotherms for DPD over CuFe/SBA-15 are presented in Fig. 8a,b. DPD adsorption is an important parameter in determining the kinetics of its heterogeneously catalyzed oxidation, and
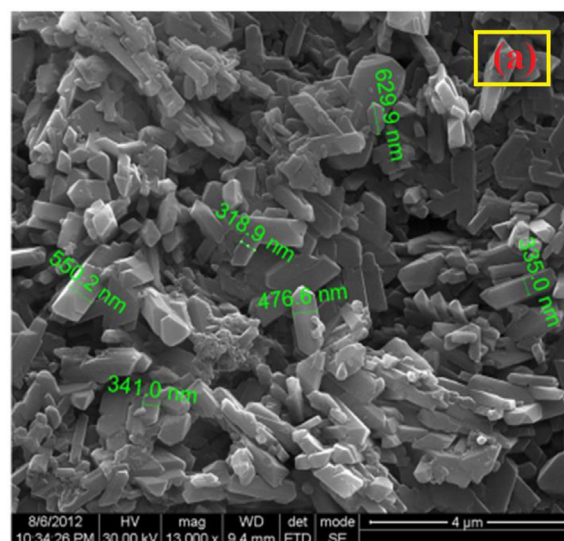
Fig. 6. (a) SEM image and (b) EDX elemental compositions of CuFe/SBA-15.

hence equilibrium constants for DPD adsorption were measured. Langmuir isotherms assume monolayer adsorption over identical, localised catalyst sites as described in Eq. (3) [37,38]

$$q_e = \frac{K_L C_e}{1 + q_M C_e} \tag{3}$$

A linear form of this expression is

$$\frac{C_e}{q_e} = \frac{1}{q_M K_L} + \frac{C_e}{q_M} \tag{4}$$

where, K$_L$ is the Langmuir equilibrium constant (L/mg), and q$_M$ (mg/g) is the monolayer adsorption capacity, which were calculated from a plot C$_e$/q$_e$ versus C$_e$ (adsorbed equilibrium concentration). The characteristic parameter of Langmuir isotherm can be illustrated in terms of dimensionless equilibrium parameter C$_e$ is the equilibrium concentration (mg/L), q$_e$ is the amount of DPD adsorbed at equilibrium (mg/g). The essential features of the Langmuir isotherm can be expressed in terms of a dimensionless constant called separation factor (R$_L$) also called known as the equilibrium parameter which is defined by the following Eq. (5),

$$R_L = \frac{1}{1 + K_L C_0} \tag{5}$$

The Freundlich isotherm is a refinement of the Langmuir approach which is better suited to inhomogeneous catalysts exhibiting a distribution of active centers which may participate in adsorption. The Freundlich isotherm is expressed as Eq. (6):

$$q_e = K_F C_e^{\frac{1}{n}} \tag{6}$$

A linear form of this expression is

$$\log q_e = \log K_F + \frac{1}{n} \log C_e \tag{7}$$

where, K$_F$ (L/g) is the Freundlich constant and n (g/L) is the Freundlich exponent. Therefore the plot of log q$_e$ versus log C$_e$ enables the constant and exponent "n" to be determined. The resulting values for DPD adsorption over CuFe/SBA-15 assuming Langmuir adsorption were q$_m$ = 13.75 mg/g and K$_L$ = 0.019 L/mg as presented
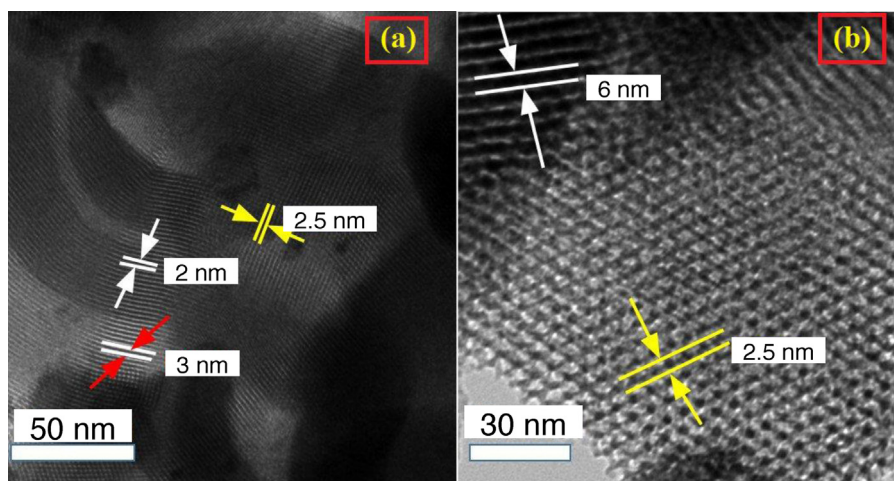
Fig. 7. HRTEM images of CuFe/SBA-15 catalyst (a) parallel and (b) perpendicular to the pore channels.
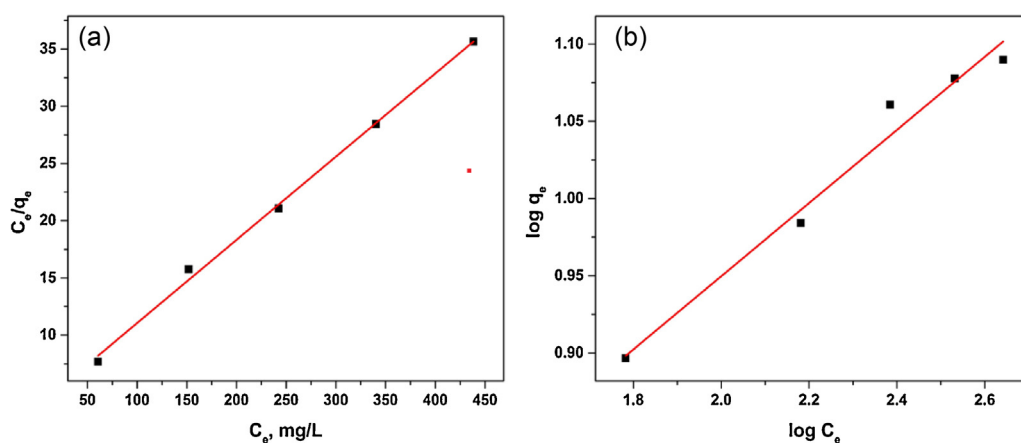

Fig. 8. (a) Langmuir isotherm or (b) Freundlich isotherm fits to DPD adsorption over CuFe/SBA-15 catalyst at 27 °C.

Table 1

Langmuir and Freundlich isotherm constants for DPD adsorption over CuFe/SBA-15.

Catalyst	Langmuir isotherm constants				Freundlich isotherm constants			
	q_m, mg/g	K_L, L/mg	R^2	R_L	$1/n$	n	K_F, L/g	R^2
CuFe/SBA-15	13.75	0.019	0.9974	0.3436–0.0947	0.237	4.2	0.322	0.9767

in Table 1. The value of R_L indicates the shape of the isotherms to be either unfavorable ($R_L >1$), linear ($R_L = 1$) or favorable ($0 < R_L > 1$). Both isotherms present similar quality fits to the experimental data, and hence we favour the simpler Langmuir parameter for CuFe/SBA-15 for adsorption at a common active site; DPD adsorption increases with increasing equilibrium concentration.

3.3. DPD degradation by CuFe/SBA-15

Experimental conditions for DPD degradation were adapted from relevant literature [31], wherein a significant excess of peroxide was employed to ensure operation in a regime where complete oxidation was possible. The solution pH was initially 4 and decreased slightly to 3.1 over the course of reaction, presumably due to the formation of acidic oxidation products. Fig. 9a shows UV–vis spectra of the DPD solution as a function of reaction time. The presence of DPD is indicated by an absorption at $\lambda_{max} = 240$ nm, which decays to around 90% of its original intensity within 120 min in the presence of CuFe/SBA-15. The degradation efficiency of CuFe/SBA-15 towards DPD relative to that of monometallic Fe/SBA-15 and Cu/SBA-15 counterparts is compared in Fig. 9b. Only 49.8% and 48.7% of DPD was oxidized over 4 wt% Cu/SBA-15 and 4 wt% Fe/SBA-15 respectively, reflecting their limited individual oxidation potential [39,40]. In contrast, the bimetallic CuFe/SBA-15 removed 83% of DPD, while a physical mixture of over 4 wt% Cu/SBA-15 and 4 wt% Fe/SBA-15 together only removed 65% of DPD, evidencing a strong synergy between Fenton and copper catalyzed DPD degradation.

As shown in Table 1, the equilibrium adsorption capacity of CuFe/BSA-15 is only 14 mg/$g_{catalyst}$, and hence adsorption can only account for 0.14% of the observed DPD loss, the overwhelming majority of which is therefore ascribed to its oxidation by hydroxyl radicals (OH$^\bullet$) generated through H_2O_2 decomposition over Cu^{2+} and Fe^{3+} active sites, resulting in mineralization of the organic contaminant to CO_2 and water[41–45]. Fig. 10a shows the influence of CuFe/SBA-15 catalyst loading on TOC removal at a fixed degradation time of 120 min and 8 mM H_2O_2 concentration. DPD decomposition was approximately first order in catalyst loading up to 100 mg/L,
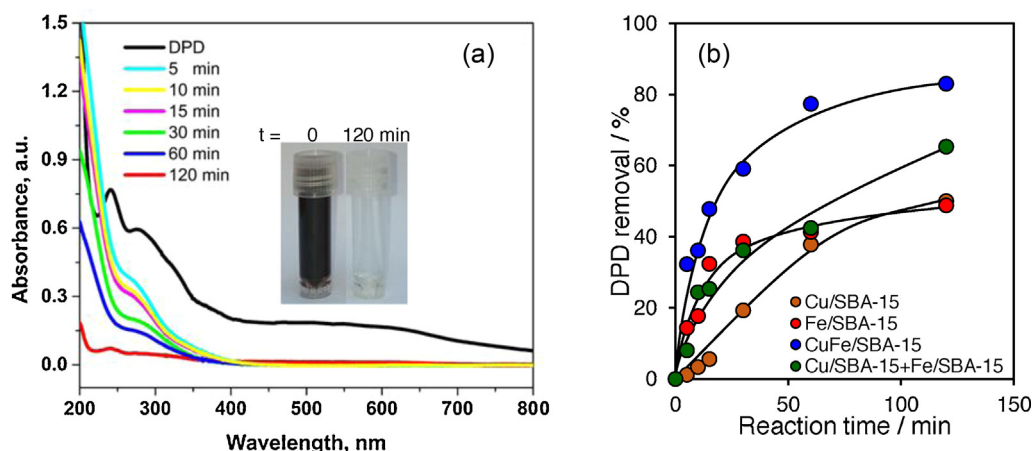
Fig. 9. (a) UV–vis spectra of DPD solution as a function of reaction time over CuFe/SBA-15, and (b) comparative DPD removal efficiency determined by DRUVS of Cu/SBA-15, Fe/SBA-15, bimetallic CuFe/SBA-15 and a physical mixture of Cu/SBA-15 + Fe/SBA-15. Reaction conditions: 100 mL water, 100 mg DPD, 10 mg catalyst, 25 °C and 8 mM H_2O_2.
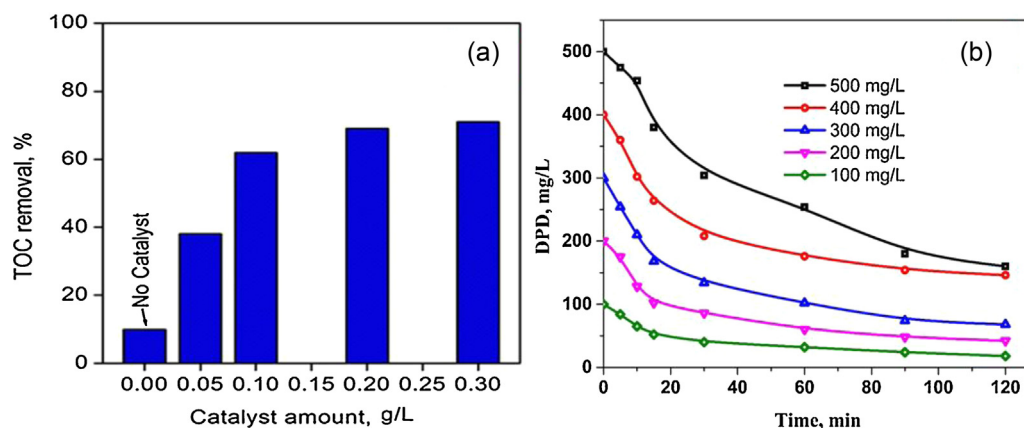

Fig. 10. (a) TOC removal after 120 min DPD oxidative degradation as a function of CuFe/SBA-15 loading, and (b) DPD concentration in solution during oxidative degradation over CuFe/SBA-15. Reaction conditions: 100 mL water, 25 °C, 8 mM H_2O_2, and (a) 100 mg DPD and (b) 10 mg catalyst.

above which little further increase in degradation rate occurred, indicating that DPD oxidation becomes mass-transport limited at high catalyst loadings[46–50]. Fig. 10b shows the rate of DPD degradation as a function of initial concentration. At low concentrations, the degradation efficiency was 85% after 120 min for 100 ppm DPD, the degradation efficiency was slightly decreased at the highest concentration. However, the initial rate of degradation (after 10 min) increased from 9.2×10^{-3} mg/min to 3.5×10^{-2} mg/min with rising initial DPD concentration from 100 to 500 mg/L. This positive reaction order in DPD suggests that adsorption is slow and may be rate-limiting in the oxidation.

FTIR spectra of the DPD solution before and after catalyst treatment (Fig. 11a,b) revealed significant changes in the organic species present, with the intensities of C−H and C−C bands [51,52] between 2800 and 3000 cm^{-1} and 1000–1500 cm^{-1} (indicative of alkyl, amine and phenyl groups) decreasing post-reaction. Atomic absorption spectroscopy of the filtrate and spent catalyst recovered after DPD degradation revealed negligible Cu and Fe leaching (<0.5 ppm and 0.2 ppm leached respectively), equating to ~2–5% of the original transition metal incorporated into the catalyst. Recycling experiments revealed that the catalyst structure (Figs. S2 and S3) was retained following DPD oxidative degradation, and that CuFe/SBA-15 could be re-used three consecutive times with negligible activity loss (Fig. S4), confirming its excellent stability. A simple cost analysis for the synthesis and application of our CuFe/SBA-15 catalyst to the remediation of a single batch of DPD contaminated water (at a relatively high level of 0.5 g/L) is pro-
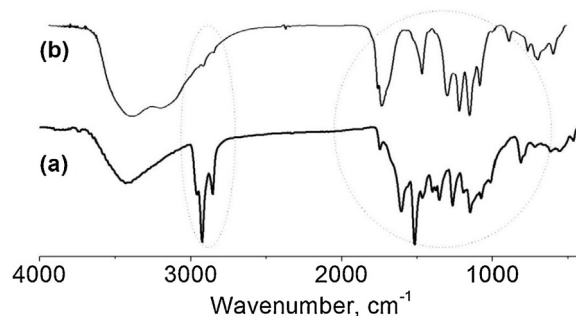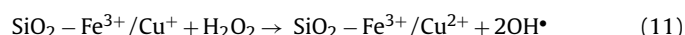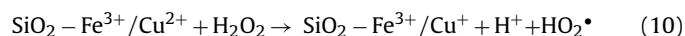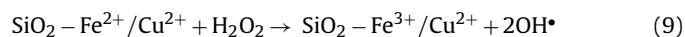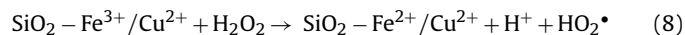

Fig. 11. FTIR spectra of (a) as-prepared, and (b) post-reaction DPD solution after treatment with CuFe/SBA-15 catalyst.

vided in Table S1, which suggests an indicative cost of US$17 for a single 100 L batch, however the excellent stability of our catalyst system suggests it can be reused at least three times, and hence the true cost is likely significantly less than US$0.05/L, rending this AOP economically viable.

3.4. Proposed mechanism for DPD degradation

Heterogeneously catalyzed Fenton oxidation is proposed to occur via the formation of surface peroxides, which dissociate to produce peroxyl radicals and in turn promote oxidative degradation of organic contaminants. DRUVS and XPS both evidence the

formation of CuO and Fe_2O_3 surface species, which must be the sites for radical formation; Fe^{3+} and Cu^{2+} sites present in CuFe/SBA-15 likely generate hydroperoxyl and hydroxyl radicals from H_2O_2 according to Eqs. (8)–(11) below [6,21,24]:

$$SiO_2 - Fe^{3+}/Cu^{2+} + H_2O_2 \rightarrow SiO_2 - Fe^{2+}/Cu^{2+} + H^+ + HO_2^\bullet \quad (8)$$

$$SiO_2 - Fe^{2+}/Cu^{2+} + H_2O_2 \rightarrow SiO_2 - Fe^{3+}/Cu^{2+} + 2OH^\bullet \quad (9)$$

$$SiO_2 - Fe^{3+}/Cu^{2+} + H_2O_2 \rightarrow SiO_2 - Fe^{3+}/Cu^+ + H^+ + HO_2^\bullet \quad (10)$$

$$SiO_2 - Fe^{3+}/Cu^+ + H_2O_2 \rightarrow SiO_2 - Fe^{3+}/Cu^{2+} + 2OH^\bullet \quad (11)$$

The slight fall in pH during reaction is consistent with the generation of protons (and organic acids) in the above reactions. In principle, either transition metal cation may undergo reduce first and hence initiate DPD oxidation, however it is likely that the synergy arises from a combination of enhanced peroxide decomposition and faster redox processes driven through the reduction of Fe^{3+} by Cu^+ [27,29] as shown in Eq. (11) the spillover of reactively-formed partial oxidation products of DPD from one metal site to the other. However, such mechanistic aspects will be the subject of future investigations. Experimental verification of the proposed catalytic cycle, which involves the reduction of Fe(III)/Cu(II) to Fe(II)/Cu(I) and subsequent re-oxidation of both transition metals, is problematic due to the transient nature of the reduced species whose lifetimes likely span ns $\rightarrow$ μs. Identification of such short-lived Fe(II)/Cu(I) species by conventional X-ray or UV–vis spectroscopies with spectral acquisition on the ms $\rightarrow$ min timescale would be hence impossible. Unequivocal evidence for low oxidation state transients would also be extremely difficult unless the catalytic cycles of every metal cation in our catalysts were precisely synchronised such that each was reduced simultaneously and then re-oxidised simultaneously (entirely unfeasible in a thermally-driven reaction); otherwise only average oxidation states could be measured. Surface silanols (Si—O—H) may also help to hydrogen bond the amine functions present within DPD, increasing the surface lifetime of the organic substrate and hence probability of reaction with proximate hydroxyl radicals formed at CuO and Fe_2O_3 nanoparticles to form smaller molecular fragments, including amines, alcohols and acids as determined by HPLC (Fig.S1), alongside CO_2 and H_2O as per Eq. (12):

$$DPD + OH^\bullet \rightarrow Organic\, fragments + CO_2 \uparrow + H_2O \quad (12)$$

4. Conclusions

A bimetallic mesoporous SBA-15 catalyst was synthesized containing highly dispersed CuO and Fe_2O_3 oxides, and applied to the oxidative degradation of N,N-diethyl-p-phenyl diamine in water. DPD adsorption was well described by Langmuir adsorption, with a maximum adsorption capacity of 13.75 mg/g at ambient temperature. Oxidative degradation of DPD at 100 mg/L occurred over CuFe/SBA-15 with 83% destruction within 120 min. The initial rate of degradation was first order in DPD for concentrations spanning 100–500 mg/L. CuFe/SBA-15 appears an excellent heterogeneous catalyst for DPD removal from aqueous solutions.

Conflict of interest

The authors declare no competing financial interest.

Acknowledgements

Appendix A. Supplementary data

Supplementary data associated with this article can be found, in the online version, at http://dx.doi.org/10.1016/j.apcatb.2016.06.040.

References

[1] S.D. Richardson, T.A. Ternes, Anal. Chem. 86 (2014) 2813–2848.
[2] N. Bolong, A.F. Ismail, M.R. Salim, T. Matsuura, Desalination 239 (2009) 229–246.
[3] A. Jurado, E. Vàzquez-Suñé, J. Carrera, M. López de Alda, E. Pujades, D. Barceló, Sci. Total Environ. 440 (2012) 82–94.
[4] M. Stuart, D. Lapworth, E. Crane, A. Hart, Sci. Total Environ. 416 (2012) 1–21.
[5] T. Deblonde, C. Cossu-Leguille, P. Hartemann, Int. J. Hyg. Environ. Health 214 (2011) 442–448.
[6] Y.J. Chan, M.F. Chong, C.L. Law, D.G. Hassell, Chem. Eng. J. 155 (2009) 1–18.
[7] L. Kovalova, H. Siegrist, U. von Gunten, J. Eugster, M. Hagenbuch, A. Wittmer, R. Moser, C.S. McArdell, Environ. Sci. Technol. 47 (2013) 7899–7908.
[8] S. Karthikeyan, D.D. Dionysiou, A.F. Lee, S. Suvitha, P. Maharaja, K. Wilson, G. Sekaran, Catal. Sci. Technol. 6 (2016) 530–544.
[9] T. Yonar, K. Kestioglu, N. Azbar, Appl. Catal. B: Environ. 67 (2006) 223–228.
[10] S. Malato, J. Blanco, A. Vidal, C. Richter, Appl. Catal. B: Environ. 37 (2002) 1–15.
[11] E. Neyens, J. Baeyens, J. Hazard. Mater. 98 (2003) 33–50.
[12] D. Zhao, J. Feng, Q. Huo, N. Melosh, G.H. Fredrickson, B.F. Chmelka, G.D. Stucky, Science 279 (1998) 548–552.
[13] Z. Wu, D. Zhao, Chem. Commun. 47 (2011) 3332–3338.
[14] Z. Dai, J. Bao, X. Yang, H. Ju, Biosens. Bioelectron. 23 (2008) 1070–1076.
[15] M. Hartmann, S. Kullmann, H. Keller, J. Mater. Chem. 20 (2010) 9002–9017.
[16] T. Shahwan, S. Abu Sirriah, M. Nairat, E. Boyacı, A.E. Eroğlu, T.B. Scott, K.R. Hallam, Chem. Eng. J. 172 (2011) 258–266.
[17] S.-P. Sun, A.T. Lemley, J. Mol. Catal. A: Chem. 349 (2011) 71–79.
[18] N. Panda, H. Sahoo, S. Mohapatra, J. Hazard. Mater. 185 (2011) 359–365.
[19] L. Luo, C. Dai, A. Zhang, J. Wang, M. Liu, C. Song, X. Guo, Catal. Sci. Technol. 5 (2015) 3159–3165.
[20] F. Martínez, G. Calleja, J.A. Melero, R. Molina, Appl. Catal. B: Environ. 70 (2007) 452–460.
[21] P. Shukla, S. Wang, H. Sun, H.-M. Ang, M. Tadé, Chem. Eng. J. 164 (2010) 255–260.
[22] P. Shukla, H. Sun, S. Wang, H.M. Ang, M.O. Tadé, Catal. Today 175 (2011) 380–385.
[23] R. Mellaerts, C.A. Aerts, J.V. Humbeeck, P. Augustijns, G.V. den Mooter, J.A. Martens, Chem. Commun. (2007) 1375–1377.
[24] A. Galarneau, D. Desplantier-Giscard, F. Di Renzo, F. Fajula, Catal. Today 68 (2001) 191–200.
[25] Z.-H. Lu, J. Li, A. Zhu, Q. Yao, W. Huang, R. Zhou, R. Zhou, X. Chen, Int. J. Hydrogen Energy 38 (2013) 5330–5337.
[26] Á. Szegedi, M. Popova, K. Lázár, S. Klébert, E. Drotár, Microporous Mesoporous Mater. 177 (2013) 97–104.
[27] Y. Wang, H. Zhao, G. Zhao, Appl. Catal. B: Environ. 164 (2015) 396–406.
[28] J.A. Melero, G. Calleja, F. Martínez, R. Molina, Catal. Commun. 7 (2006) 478–483.
[29] Z. Han, Y. Dong, S. Dong, J. Hazard. Mater. 189 (2011) 241–248.
[30] P. Nagaraja, A. Shrestha, A. Shivakumar, A. Gowda, Use of N,N-diethyl-p-phenylenediamine sulphate for the spectrophotometric determination of some phenolic and amine drugs, Acta Pharm. (2010) 217.
[31] M.P. Pachamuthu, S. Karthikeyan, G. Sekaran, R. Maheswari, A. Ramanathan, CLEAN – Soil Air Water 43 (2015) 375–381.
[32] Y. Morita, K. Suzuki, A. Yagami, M. Isami, A. Sano, Y. Yokoyama, K. Matsunaga, Contact Dermatitis 69 (2013) 118–119.
[33] S. Shylesh, A.P. Singh, J. Catal. 244 (2006) 52–64.
[34] X. Zhong, J. Barbier Jr., D. Duprez, H. Zhang, S. Royer, Appl. Catal. B: Environ. 121–122 (2012) 123–134.
[35] M.P. Pachamuthu, V.V. Srinivasan, R. Maheswari, K. Shanthi, A. Ramanathan, Catal. Sci. Technol. 3 (2013) 3335–3342.
[36] S. Karthikeyan, C.J. Magthalin, A.B. Mandal, G. Sekaran, RSC Adv. 4 (2014) 19183–19195.
[37] S. Nethaji, A. Sivasamy, G. Thennarasu, S. Saravanan, J. Hazard. Mater. 181 (2010) 271–280.
[38] C.-H. Huang, K.-P. Chang, H.-D. Ou, Y.-C. Chiang, C.-F. Wang, Microporous Mesoporous Mater. 141 (2011) 102–109.
[39] V. Subbaramaiah, V.C. Srivastava, I.D. Mall, AIChE J. 59 (2013) 2577–2586.
[40] F.L.Y. Lam, A.C.K. Yip, X. Hu, Ind. Eng. Chem. Res. 46 (2007) 3328–3333.
[41] S. Karthikeyan, R. Boopathy, G. Sekaran, J. Colloid Interface Sci. 448 (2015) 163–174.
[42] I. Ursachi, A. Stancu, A. Vasile, J. Colloid Interface Sci. 377 (2012) 184–190.
[43] S. Karthikeyan, G. Sekaran, Phys. Chem. Chem. Phys. 16 (2014) 3924–3933.

[44] S. Karthikeyan, A. Titus, A. Gnanamani, A.B. Mandal, G. Sekaran, Desalination 281 (2011) 438–445.
[45] D.Q. Khieu, D.T. Quang, T.D. Lam, N.H. Phu, J.H. Lee, J.S. Kim, J. Inclusion Phenom. Macrocyclic Chem. 65 (2009) 73–81.
[46] N.A. Hamill, L.R. Weatherley, C. Hardacre, Appl. Catal. B: Environ. 30 (2001) 49–60.
[47] C.A. Martinez-Huitle, S. Ferro, Chem. Soc. Rev. 35 (2006) 1324–1340.
[48] R. Levi, M. Milman, M.V. Landau, A. Brenner, M. Herskowitz, Environ. Sci. Technol. 42 (2008) 5165–5170.

[49] E. Kan, S.G. Huling, Environ. Sci. Technol. 43 (2009) 1493–1499.
[50] Y.G. Adewuyi, Environ. Sci. Technol. 39 (2005) 8557–8570.
[51] S. Kumar, S. Tonda, B. Kumar, A. Baruah, V. Shanker, J. Phys. Chem. C 117 (2013) 26135–26143.
[52] J.C. Manayil, C.V.M. Inocencio, A.F. Lee, K. Wilson, Green Chem. 18 (2016) 1387–1394.